

Structural analysis of Er silicide nanowires on Si(001) using three-dimensional medium-energy ion scattering

Takane Kobayashi*

RIKEN (The Institute of Physical and Chemical Research), 2-1 Hirosawa, Wako, Saitama 351-0198, Japan

(Received 5 December 2006; revised manuscript received 31 January 2007; published 1 March 2007)

Er silicide nanostructures were produced by depositing Er on a clean Si(001) substrate. From the off-line observation by scanning electron microscopy, several kinds of nanostructures were observed; nanowires, nanobelts made by a lateral binding of nanowires, and three-dimensional (3D) islands. The 3D islands occupied a major part in those nanostructures, and had slight beltlike structures on their surfaces. The three-dimensional medium-energy ion scattering clearly indicated that the nanostructures were highly epitaxial, and that the nanostructures had a single kind of crystallographic structure of monoclinic ErSi_2 , deformed from hexagonal.

DOI: [10.1103/PhysRevB.75.125401](https://doi.org/10.1103/PhysRevB.75.125401)

PACS number(s): 68.65.-k, 68.49.Sf, 71.20.Eh

I. INTRODUCTION

A great deal of research on nanostructures has been carried out for a long time.¹⁻³ When materials width and/or height become comparable to characteristic dimensions (e.g., electronic wavelength or magnetic domain width), new physical properties are expected to appear, which may lead to a production of future electronic, optoelectronic, and magnetic devices.⁴⁻⁶

The strain in the epitaxially grown nanomaterials, induced by matching to the periodicity of the substrate lattice may also give rise to the new physical properties. It has been found that strained Si nanofilms epitaxially grown on a substrate of SiGe have a large carrier mobility in the direction of tensile stress compared with usual not-strained Si films.⁷

STM is the sensitive tool to observe the surface structure of nanomaterials. However, their structures of vertical to substrate surfaces cannot be studied by STM.

Three-dimensional medium-energy ion scattering (3D-MEIS) is a promising tool for analyzing the crystallographic structure of nanomaterials.^{8,9} It enables, by time-of-flight (TOF) spectroscopy, to measure scattering intensities from different depths and elements, at one measuring run. Therefore, the scattering intensity pattern for the element in the nanostructure is compared with those for the element in the substrate. Thus, the three-dimensional crystallographic structure of the materials with the thickness of nanometers is clearly obtained and elucidated.

A 3D-MEIS system has been recently developed and applied to the crystallographic analysis of Er silicide nanofilms grown on Si(111).⁸ In the present paper, a 3D-MEIS analysis on Er silicide nanostructures produced by depositing a small amount of Er on Si(001) is reported, together with an off-line scanning electron microscopy (SEM) observation. The 3D-MEIS analysis has revealed that the crystallographic structure of the Er silicide nanostructures is not hexagonal with a sixfold symmetry of rotation in the Er atomic planes vertical to the Si(001), but monoclinic with a twofold symmetry of rotation. The structure is strained also in the planes vertical to the substrate surface.

II. EXPERIMENTS

A. Sample preparation

A sample preparation was performed in an ultrahigh vacuum system with a base pressure of 1×10^{-10} Torr. The Si(001) sample was *n*-type wafer ($1 \Omega \text{ cm}$), chemically cleaned, and then was outgassed by heating to 600°C . After being outgassed, it was flashed briefly at 1200°C to remove surface oxide, and then cooled to room temperature. The temperatures of the sample were measured using an optical pyrometer. Er was evaporated from an electron beam evaporator. The sample was prepared by the deposition of about 1.5 monolayers (ML) ($1 \text{ ML} = 6.78 \times 10^{14} \text{ atoms/cm}^2$) Er on the Si(001) substrate. The chamber pressure remained below 1×10^{-8} Torr during evaporation. It took 1 hour for the deposition and during the deposition the substrate temperature was kept at 620°C . After the deposition, the sample was post heated at the same temperature for 30 minutes.

B. Scattered particle detection

Details of 3D-MEIS spectroscopy were described elsewhere.⁸⁻¹⁰ In brief, the system is characterized as follows: a pulsed He^+ ion beam with an energy of 100 keV is used for an incident beam. Three-dimensional spectroscopy is possible by using a position-sensitive (two-dimensional) and time-resolving (additional third-dimensional) MCP detector with two delay-line anodes wound perpendicular to each other (RoentDek DLD120).¹¹

The pulsed He^+ ion beam has a full pulse width of 1.3 ns and a repetition rate of 50 kHz. The time resolution of the 3D-MEIS system is evaluated to be 1.3 ns. The energy resolution converted from the flight times of scattered particles depends on flight time. For example, the energy resolution of the particles scattered from surface Si and Er atoms is calculated to be 0.012 and 0.014, respectively, in the present experiment. Typically, depth resolution is 2 nm for Er disilicide.¹² The scattering angle at the center of the detector is 120° . The diameter of the MCP detector is 120 mm and the distance from the sample to the center of the detector is 190 mm. The range of the measurable scattering angle is $\pm 17.5^\circ$.

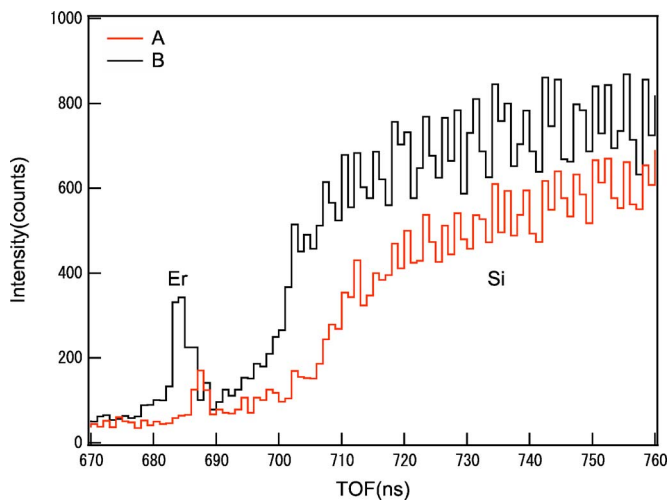


FIG. 1. (Color online) TOF spectra of He particles scattered from the Er silicide and the Si(001) substrate. The spectra A and B were obtained at the different scattering angles. The spectra in the flight time ranges of 681–689 ns and 700–760 ns correspond to Er and Si atoms, respectively.

III. EXPERIMENTAL RESULTS

A. Time-of-flight spectra and three-dimensional medium-energy scattering images

Figure 1 shows the TOF spectra of He particles scattered to different angles. Since the scattering angle for spectrum A is smaller than that for B, the rising time of spectrum A is smaller than that for B. The intensities in the flight time ranges of 681–689 ns and 700–760 ns of spectra A and B are due to He particles scattered by Er and Si atoms, respectively. From the width of the spectral peak of Er, the average thickness of the Er silicide is calculated to be 4.6 nm.¹²

Figures 2(a) and 2(b) show, respectively, the scattering patterns due to Si and Er atoms obtained from the analyses of TOF spectra at all scattering angles covered by the MCP, where Si atoms located at the depth of 14–60 nm and all of Er atoms have been taken into account, respectively. The horizontal and the vertical axes indicate the scattered angle with respect to the normal to Si(001), θ_2 , and the deflection angle with respect to Si $\{1\bar{1}0\}$, ϕ , respectively. The scattered angle θ_2 is related to the scattering angle θ by the equation $\theta = 180^\circ - (\theta_1 + \theta_2)$, where θ_1 is the incident angle of the pulsed ion beam with respect to the surface normal. The color bar drawn at the upper side of each image indicates the intensity of scattered He particles at each pixel. White corresponds to high intensity and blue to low.

In Fig. 2(a), clear dark stripes of low yield regions of the intensities scattered from Si atoms are observed, and dark ones for Er atoms are also observed in Fig. 2(b), although less clear. These dark stripes represent the blocking cone aggregations by Si and Er atom planes, respectively. The stripes for Er atom represent that Er silicides are produced with crystallographic regularity. At the deflection angle of $\phi = 0^\circ$ with respect to Si $\{1\bar{1}0\}$, we can see the dark stripes due to both Si and Er, as shown in Figs. 2(a) and 2(b). They are blocking cone aggregations by Si $\{1\bar{1}0\}$ and by Er atom

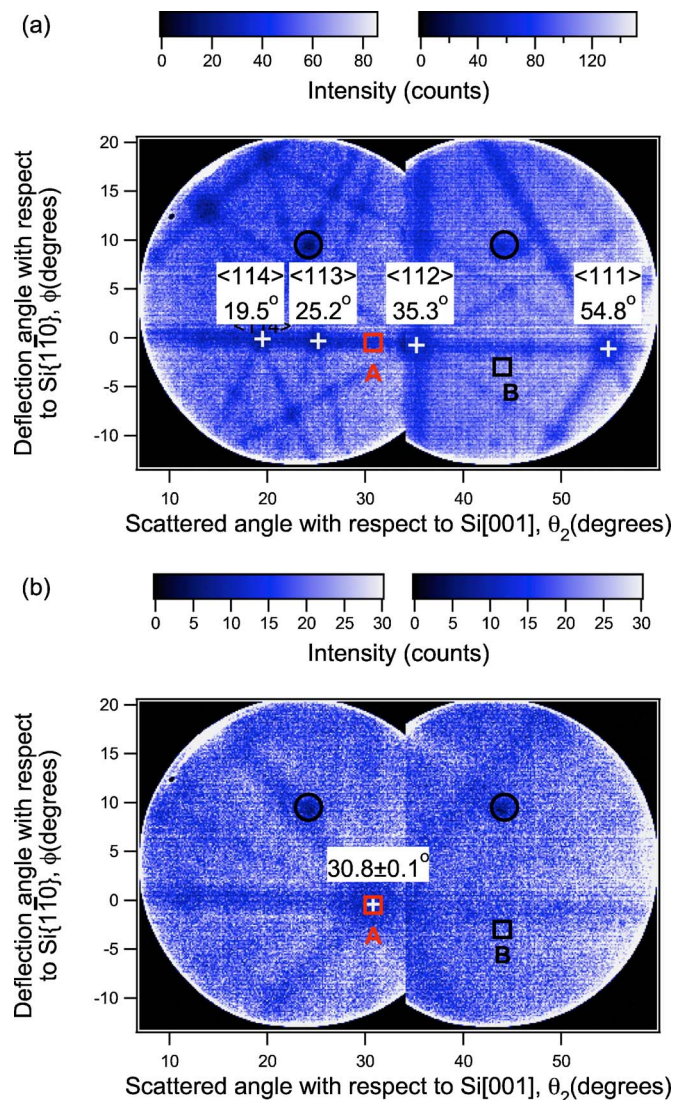


FIG. 2. (Color online) Intensity distribution of He particles scattered around Si $\{1\bar{1}0\}$ plane. (a) Scattering by Si atoms at the depth of 16–60 nm in the substrate. (b) Scattering by Er atoms. The horizontal and the vertical axes in both figures, represent the scattered angle with respect to the normal to Si(001), θ_2 , and the deflection angle with respect to Si $\{1\bar{1}0\}$, ϕ , respectively.

planes parallel to Si $\{1\bar{1}0\}$ planes, respectively. We can also see the dark spots on these stripes. They are, respectively, blocking cones due to Si atomic axes on Si $\{1\bar{1}0\}$, and Er atomic axes on the Er atom planes concerned. In Fig. 2(a), main blocking cones due to Si axes on the Si $\{1\bar{1}0\}$ are observed at the scattered angles $\theta_2 = 19.5, 25.2, 35.3,$ and 54.8° . They can be indexed to Si axes of $\langle 114 \rangle$, $\langle 113 \rangle$, $\langle 112 \rangle$, and $\langle 111 \rangle$, respectively. In Fig. 2(b), one clear blocking cone due to Er atom axes on the Er atom planes parallel to Si $\{1\bar{1}0\}$ is observed at $\theta_2 = 30.8 \pm 0.1^\circ$.

Blocking cones were searched also around Si $\{1\bar{1}0\}$ which is at an angle of 45° with respect to the Si $\{1\bar{1}0\}$. In Fig. 3, ϕ is the deflection angle with respect to Si $\{1\bar{1}0\}$. Figure 3(a) shows the blocking pattern due to Si atoms, in the range of

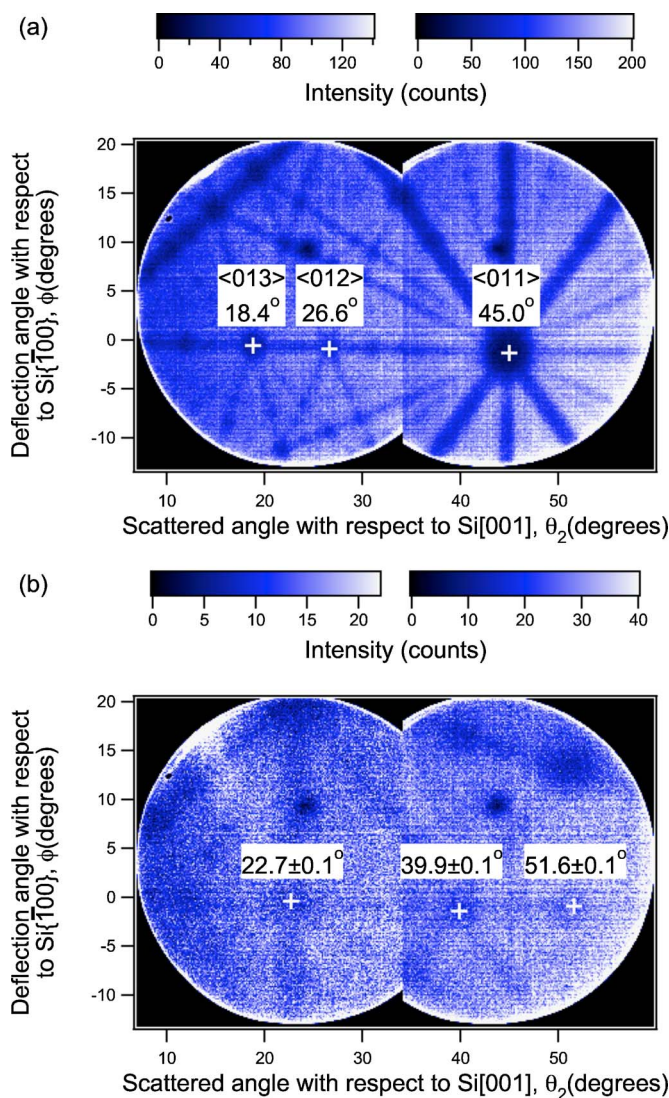


FIG. 3. (Color online) Intensity distribution of He particles scattered around $\text{Si}\{\bar{1}00\}$ plane. (a) Scattering by Si atoms at the depth of 16–60 nm in the substrate. (b) Scattering by Er atoms. The horizontal and the vertical axes are the same as in Fig. 2.

θ_2 from 10° to 60° . Besides the blocking cone aggregation by $\text{Si}\{\bar{1}00\}$, clear blocking cones due to Si axes on the $\text{Si}\{\bar{1}00\}$ plane are observed at $\theta_2 = 18.4^\circ$, 26.6° , and 45.0° . They can be indexed, respectively, to the Si axes of $\langle 013 \rangle$, $\langle 012 \rangle$, and $\langle 011 \rangle$. Figure 3(b) shows the blocking pattern due to He particles scattered from Er atoms observed around $\text{Si}\{\bar{1}00\}$. The aggregation of blocking cones (slightly dark stripe at the deflection angle $\phi = 0^\circ$) due to Er atomic planes parallel to $\text{Si}\{\bar{1}00\}$ is observed. Therefore, it is revealed that there are also Er atomic planes parallel to $\text{Si}\{\bar{1}00\}$. Further, blocking cones by Er atom axes on the Er atomic planes concerned are observed at $\theta_2 = 22.7 \pm 0.1^\circ$, $39.9 \pm 0.1^\circ$, and $51.6 \pm 0.1^\circ$.

Low yield areas indicated by solid circles in Figs. 2(a) and 2(b) are observed, and are also at the same positions in Figs. 3(a) and 3(b). These are not due to the real blocking cones, but are produced because scattered particles pass through the channels of the front MCP without collisions to

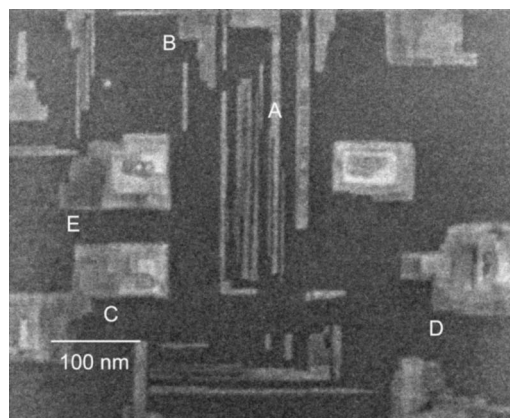


FIG. 4. SEM image of the morphological structure of Er silicide analyzed by 3D-MEIS. Nanowires, nanobelts and 3D islands are visible.

its wall. Such dark spots were ignored for the structural analysis.

B. Scanning electron microscopy observation

After the analysis by 3D-MEIS, the morphology of the sample was observed by off-line SEM. The SEM image is shown in Fig. 4. Several structures of nanowires (marked by A), nanobelts of bundles of such nanowires (marked by B), and 3D islands (marked by C, D, E) are seen to be dispersed at various places.

The growth directions of these nanowires are parallel to $\text{Si}\langle 1\bar{1}0 \rangle$ or $\text{Si}\langle \bar{1}10 \rangle$ directions, which are the same as those in the STM observation by Chen *et al.*^{2,8} Therefore it is considered that the Er silicide (ErSi_2) nanowires obtained in the present experiment are epitaxial ones similar to those produced in the experiment by Chen *et al.*, although the widths of the present nanowires are larger than those produced by them. Nanobelts are formed by the contact of nanowires after growing of the widths of them. We can see nanobelt structures made from a few nanowires, as shown by mark A. Regarding the planar structure marked by B, the planar combination is much progressed and the borders between nanowires are only slightly observed.

It can be seen that the 3D islands occupy a large part in the SEM image. When we consider that these 3D islands are thicker than those of nanowires and nanobelts, we can presume that Er signals in TOF spectra will come out mainly from those islands. Beltlike structures are very faintly visible on the islands, and it can be assumed that these islands are formed by the 3D pile up of nanobelts. According to the STM observation of islands by other authors, similar pile up was also seen at the process of island formation.¹³ Therefore, it can be expected that their crystallographic structures may keep the same ones as those of nanobelts, or nanowires.

IV. STRUCTURE MODEL OF Er SILICIDE NANOSTRUCTURES

The crystallographic structure model of the Er silicide nanostructures is presented here, as shown in Figs. 5(a) and

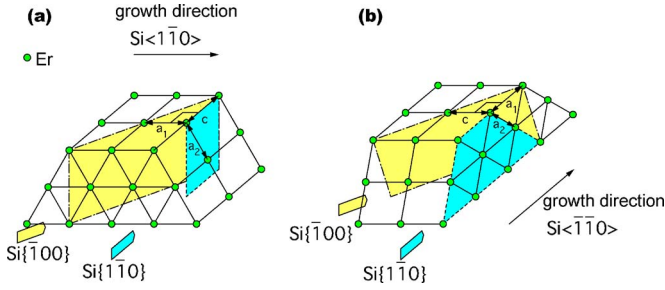


FIG. 5. (Color online) Schematic of the crystallographic structure model of ErSi_2 nanostructures. Er atomic planes parallel to $\text{Si}\{1\bar{1}0\}$ are shown by the two kinds of blue colored areas in (a) and (b). Er atomic planes parallel to $\text{Si}\{100\}$ are shown by one kind of yellow colored area.

5(b). The 3D islands are considered to be formed by the 3D pile up of nanowires and/or nanobelts. Therefore, their structure would be similar to that of the nanowire. According to the STM observation by Chen *et al.*,² the structure model is that the a_1 and c axes of the hexagonal ErSi_2 unit cell are parallel to $\text{Si}(001)$ and that a_1 axis is parallel to the growth direction of $\text{Si}\langle 1\bar{1}0 \rangle$ or $\text{Si}\langle \bar{1}10 \rangle$, but c axis is perpendicular to the direction. In the present model also, the epitaxial growth conditions for a_1 and c axes are adopted, but the hexagonal model that $a_1 = a_2$ is not, in order to make the present model consistent with the experiment.

The Er atomic planes giving rise to the blocking aggregation at $\varphi = 0$ in Fig. 2(b), i.e., those planes parallel to $\text{Si}\{1\bar{1}0\}$, are shown by the blue-colored planes in Figs. 5(a) and 5(b). The other Er atomic planes giving rise to the blocking aggregation at $\varphi = 0$ in Fig. 3(b), i.e., those planes parallel to $\text{Si}\{100\}$, are shown by the yellow-colored planes in Figs. 5(a) and 5(b). The angle between these two Er atomic planes is equal to the angle between $\text{Si}\{1\bar{1}0\}$ and $\text{Si}\{100\}$, and is 45° . This angle means that $a_1 = c$, which is incorporated in the present model, as shown in Figs. 5(a) and 5(b).

The Er atomic axes on the Er atomic planes parallel to $\text{Si}\{1\bar{1}0\}$, inducing the blocking cones obtained in Fig. 2(b) are depicted in Figs. 6(a) and 6(b). The fact that the two different axes induce the blocking cones at the same angle of $\theta_2 = 30.8 \pm 0.1^\circ$ gives rise to the condition $a_1 = c$, which also supports the present model. Further, from the value $\tan(30.8 \pm 0.1^\circ)$, the equation $a_2 = (0.976 \pm 0.003)a_1$ is de-

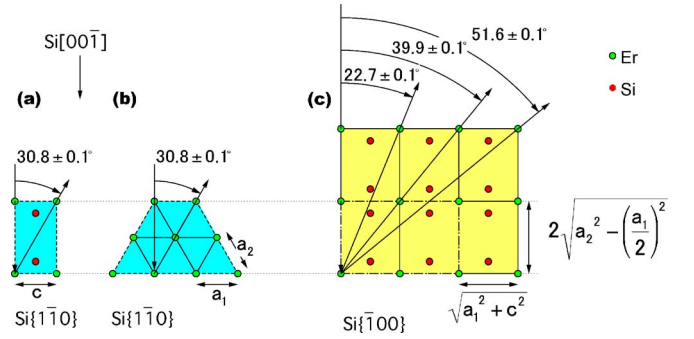


FIG. 6. (Color online) Schematic of Er atomic arrangement suspected to give the blocking cones as observed in Figs. 2 and 3. (a), (b) Planes parallel to $\text{Si}\{1\bar{1}0\}$. (c) Plane parallel to $\text{Si}\{100\}$.

duced. The Er atomic axes on the Er atomic planes parallel to $\text{Si}\{100\}$, inducing the blocking cones obtained in Fig. 3(b) are shown by the yellow-colored planes in Figs. 6(c). From the angles of the blocking cones at $22.7 \pm 0.1^\circ$, $39.9 \pm 0.1^\circ$, and $51.6 \pm 0.1^\circ$, it is also deduced the equation $a_2 = (0.981 \pm 0.003)a_1$, when the condition $a_1 = c$ is assumed. Therefore, it is concluded that $a_2 = 0.979a_1$ is deduced on an average.

Values of θ_2 shown in Figs. 6(a)–6(c) are listed in Table I together with those given by the epitaxially grown hexagonal ErSi_2 model. The observed angles and those deduced from the hexagonal model are clearly different. The crystallographic structure is surely monoclinic rather than hexagonal. The lengths of the a_1 and c axes are considered to be equal to the atomic distance on ideal $\text{Si}(001)$ surface (a), $a = 0.384$ nm. The length of the a_2 axis is calculated to be 0.376 nm. The angle γ between a_1 - and a_2 -axes is calculated to be 120.7° , which gives rise to the existence of two kinds of Er-Er atomic axes in the plane perpendicular to the c axis, as well as two kinds of Si-Si and Er-Si interatomic distances. Such monoclinic structure breaking the sixfold symmetry of rotation may give rise to interesting magnetic or electric properties, because those properties are sensitively dependent on the conduction band structure which is influenced by the structural arrangement of constituent atoms.¹⁴

V. CONCLUSION

A sample of Er silicide has been produced by depositing Er metal on a $\text{Si}(001)$ substrate kept at 620°C . The morpho-

TABLE I. Comparison of the scattered angles θ_2 of observed Er atom blocking cones with those given by the epitaxially grown hexagonal ErSi_2 model.

	Scattered angles θ_2 of observed blocking cones due to Er atoms ($^\circ$)	Scattered angles θ_2 expected from the hexagonal ErSi_2 model ($^\circ$)
$\text{Si}\{1\bar{1}0\}$	30.8 ± 0.1	30.0
$\text{Si}\{100\}$	22.7 ± 0.1	22.2
$\text{Si}\{\bar{1}00\}$	39.9 ± 0.1	39.2
$\text{Si}\{\bar{1}00\}$	51.6 ± 0.1	50.8

logical and the crystallographic structures of the Er silicide have been investigated by using SEM and 3D-MEIS. Various kinds of nanostructures (nanowire, nanobelt, and 3D island) were observed by SEM. The growth directions of the nanowires are the same as those observed in the experiment by Chen *et al.* It is observed in the present experiment that the nanobelts are formed by planar binding of nanowires. The faint structures visible on the surface of the 3D islands indicate that those islands are formed by the 3D pile up of nanowires and/or nanobelts. From the SEM image, it is probable that a large part of the Er signal originates from those 3D islands. The blocking cones observed in the 3D-MEIS images have been compared with the structure model of epitaxially grown Er silicide. It has been confirmed also for 3D island silicide the usual epitaxial growth condition of nanowires; a_1 and c axes of the unit cell are parallel to Si(001), a_1 is parallel to the nanowire growing direction of Si $\langle 1\bar{1}0 \rangle$ or

Si $\langle \bar{1}\bar{1}0 \rangle$, c is perpendicular to the growth direction, and $a_1 = c$. However, the new finding is that a_2 is not equal to a_1 , i.e., $a_2 = 0.979 a_1$, which means the unit cell is monoclinic rather than hexagonal. A similar strain in the plane vertical to the substrate surface was also found for the Er silicide epitaxially grown on Si(111). Such strains may be induced for many kinds of epitaxially grown nanomaterials. It has been proved that 3D-MEIS is a promising tool for crystallographic analysis of nanomaterials.

ACKNOWLEDGMENTS

The author would like to thank S. Shimoda, Y. Oe, Y. Nakai, Y. Yamazaki, and A. Koyama for technical support and helpful discussions, and M. Shibata and N. Akiyama, JEOL members, for the SEM observation.

-
- *Corresponding author. Electronic address: tkoba@riken.jp
¹S. M. Prokes and K. L. Wang, MRS Bull. **24**, 13 (1999).
²Y. Chen, D. A. A. Ohlberg, and R. S. Williams, J. Appl. Phys. **91**, 3213 (2002).
³Y. Chen, D. A. A. Ohlberg, G. Medeiros-Ribeiro, Y. A. Chang, and R. S. Williams, Appl. Phys. Lett. **76**, 4004 (2000).
⁴M. Sundaram, S. A. Chalmers, P. F. Hopkins, and A. C. Gossard, Science **254**, 1326 (1991).
⁵D. D. Awschalom and D. P. DiVincenzo, Phys. Today **48** (4), 43 (1995).
⁶K. Nishiguchi and S. Oda, J. Appl. Phys. **92**, 1399 (2002).
⁷S. Takagi, J. L. Hoyt, J. J. Welser, and J. F. Gibbons, J. Appl.

- Phys. **80**, 1567 (1996).
⁸S. Shimoda and T. Kobayashi, J. Appl. Phys. **96**, 3550 (2004).
⁹T. Kobayashi, Nucl. Instrum. Methods Phys. Res. B **249**, 266 (2006).
¹⁰S. Shimoda and T. Kobayashi, Nucl. Instrum. Methods Phys. Res. B **219-220**, 573 (2004).
¹¹<http://www.roentdek.com/>
¹²J. F. Ziegler, in *The Stopping and Ranges of Ions in Matter* (Pergamon, New York, 1977), Vol. 4.
¹³B. Z. Liu and J. Nogami, J. Appl. Phys. **93**, 593 (2003).
¹⁴R. A. Cowley, Physica B **350**, 1 (2004).